

Received 5 April 2017  
Accepted 4 May 2017

Edited by K. Chapman, Argonne National Laboratory, USA

**Keywords:** ball milling; 3D printing; *in situ* powder diffraction.

**Supporting information:** this article has supporting information at [journals.iucr.org/j](http://journals.iucr.org/j)

## 3D-printed jars for ball-milling experiments monitored *in situ* by X-ray powder diffraction

Nikolay Tumanov,<sup>a,b</sup> Voraksmý Ban,<sup>a,c</sup> Agnieszka Poulaïn<sup>d</sup> and Yaroslav Filinchuk<sup>a\*</sup>

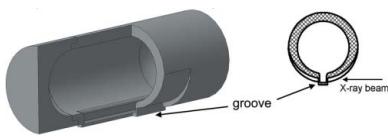
<sup>a</sup>Institute of Condensed Matter and Nanosciences, Université catholique de Louvain, place L. Pasteur, Louvain-la-Neuve, 1348, Belgium, <sup>b</sup>Department of Chemistry, University of Namur, rue de Bruxelles 61, Namur, 5000, Belgium, <sup>c</sup>MS Group, Swiss Light Source, Paul Scherrer Institute, Villigen – PSI, 5232, Switzerland, and <sup>d</sup>European Synchrotron Radiation Facility, 71 avenue des Martyrs, CS 40220, Grenoble Cedex 9, 38043, France. \*Correspondence e-mail: [yaroslav.filinchuk@uclouvain.be](mailto:yaroslav.filinchuk@uclouvain.be)

Mechanochemistry is flourishing in materials science, but a characterization of the related processes is difficult to achieve. Recently, the use of plastic jars in shaker mills has enabled *in situ* X-ray powder diffraction studies at high-energy beamlines. This paper describes an easy way to design and manufacture these jars by three-dimensional (3D) printing. A modified wall thickness and the use of a thin-walled sampling groove and a two-chamber design, where the milling and diffraction take place in two communicating volumes, allow for a reduced background/absorption and higher angular resolution, with the prospect for use at lower-energy beamlines. 3D-printed polylactic acid jars show good mechanical strength and they are also more resistant to solvents than jars made of polymethyl methacrylate. The source files for printing the jars are available as supporting information.

### 1. Introduction

Mechanochemistry is a widespread synthesis technique in all areas of chemistry (Huot *et al.*, 2013; Boldyreva, 2013; May & Moore, 2013; Zhu *et al.*, 2013; Wang, 2013; Ralphs *et al.*, 2013; Margetic & Štrukil, 2016). Various materials have been synthesized by this technique when the classical wet chemistry route was not satisfactory. However, the characterization of the reaction mixture in mechanochemistry is much less accessible than in solutions. Recently, *in situ* observations of a mechanochemical reaction were achieved by X-ray diffraction (Friščić *et al.*, 2013; Halasz, Kimber *et al.*, 2013) and by Raman spectroscopy (Gracin *et al.*, 2014). For the first time solid-state reactions were directly tracked, revealing phase transitions and other material transformations during synthesis in a ball-mill jar. Friščić's group (Friščić *et al.*, 2013) were pioneers in the field of *in situ* ball-milling experiments; they were able to observe a mechanochemical reaction by probing the entire milling container of a shaker mill device with synchrotron radiation (Fig. 1). This technique has become increasingly popular in different fields of mechanochemistry (Batzdorf *et al.*, 2015; Užarević *et al.*, 2015; Halasz, Puškarić *et al.*, 2013; Fischer, Heidrich *et al.*, 2016; Fischer, Lubjuhn *et al.*, 2016).

As the X-rays go through the entire jar, the diffraction patterns present a high background due to the scattering from the thick walls of the jar (the thick walls are necessary to ensure the integrity of the jars upon mechanical impact). Also, broad diffraction peaks are expected from the sample as a result of probing a large sample area covering the entire jar. In practice, diffraction peaks appear as doublets as the material



© 2017 International Union of Crystallography

sticks at the opposite walls of the jar, characterized by different sample-to-detector distances. An extra complexity arises from diffraction on the milling balls. This can be circumvented by finding appropriate shaking frequencies allowing for stable trajectories of the milling balls and thus making it possible to probe the space where they are not present. As a result, neither the experiment nor the analysis of the diffraction patterns is straightforward. Here we show that all these issues can be resolved by modifying the geometry and material of the milling jars.

The material of the milling jar has to satisfy certain requirements: first, it should be robust enough to withstand the impacts from the grinding balls; second, it should minimize absorption and produce a small background and no diffraction peaks; third, it should not interfere with the reaction; fourth, it should be resistant to solvents, if the jar is to be used for liquid-assisted grinding (LAG).

For the geometry of the milling jar, one obvious and simple improvement is to reduce the wall thickness of the jar in order to decrease its contribution to the background. However, one needs to find an acceptable compromise between low background and the mechanical strength (it should at least survive one experiment). A less obvious and more complex modification could improve the width of the diffraction peaks. The way this can be achieved can be understood by considering a simple model of the diffraction experiment, *i.e.* the incoming parallel beam is scattered by a sample, which has a thickness  $D$  along the beam direction, and then registered by a flat linear detector (see Fig. 2).

Then the projection  $d$  on the detector as a function of the scattering angle  $2\theta$  will be described as follows:  $d = D \tan(2\theta)$ . Thus, the contribution of the sample thickness to the FWHM

will substantially increase at high angles (we omit the exact equation for FWHM as a function of thickness to avoid complexity). Assume we want to obtain a powder diffraction pattern with the maximum resolution of  $0.7 \text{ \AA}$ . According to Bragg's law  $2\theta_{\text{lim}} = 2 \arcsin(2\lambda/d_{\text{lim}})$ ; hence we can calculate  $2\theta_{\text{lim}}$  needed to obtain the desired resolution of  $0.7 \text{ \AA}$  at various wavelengths. If  $\lambda = 0.15$  (high-energy X-rays), then  $2\theta_{\text{lim}} \approx 12.3^\circ$  and  $d = 0.22D$ ; and if  $\lambda = 0.7$  (moderate-energy X-rays, close to  $\text{Mo } K\alpha$ ), then  $2\theta_{\text{lim}} \approx 60^\circ$  and  $d = 1.73D$ . In a typical ball-milling experiment using  $\lambda \approx 0.7 \text{ \AA}$ ,  $D$  equals  $\sim 5 \text{ mm}$ , causing a significant peak broadening only due to the sample thickness.

Therefore, it becomes clear that the sample thickness should be reduced in order to maintain good resolution at high angles (especially important for moderate-energy X-rays); this can be done in a jar that has two separate chambers: one in which the actual ball-milling reaction occurs, and another in which the powder is measured. In order to implement this idea, we need to build a jar with a complex geometry; if we use the type of lathe or milling machine usually employed in the production of standard jars, making a jar with two separate chambers is complicated, especially at the stage of creating a prototype when introducing changes into a design should be a facile task. This is why we decided to use a three-dimensional (3D) printer for this purpose. 3D-printing technology is already well known in the crystallographic community, but it is mostly used for fabrication of molecular or crystal models (Casas & Estop, 2015; Kitson *et al.*, 2014; Scalfani & Vaid, 2014; Chen *et al.*, 2014).

Herein we propose different jar designs made with a 3D printer. We will show how this useful production tool can quickly make a sophisticated object on demand without compromising its quality.

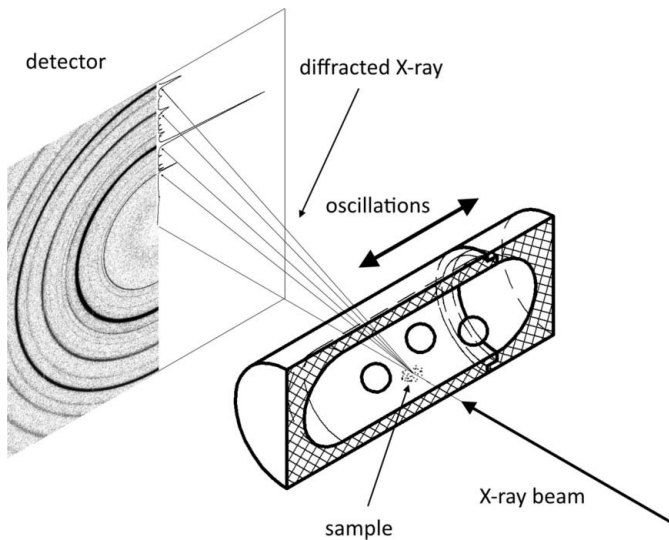


**Figure 1**

Scheme of an *in situ* ball-milling experiment monitored by powder X-ray diffraction using a shaker mill. The X-ray beam goes through the bottom of the oscillating plastic jar containing the sample and metal or ceramic balls. Diffracted X-rays are registered by one dimension of the two-dimensional detector. The orientation and oscillation of the jar could be vertical or horizontal depending on the exact experimental setup.

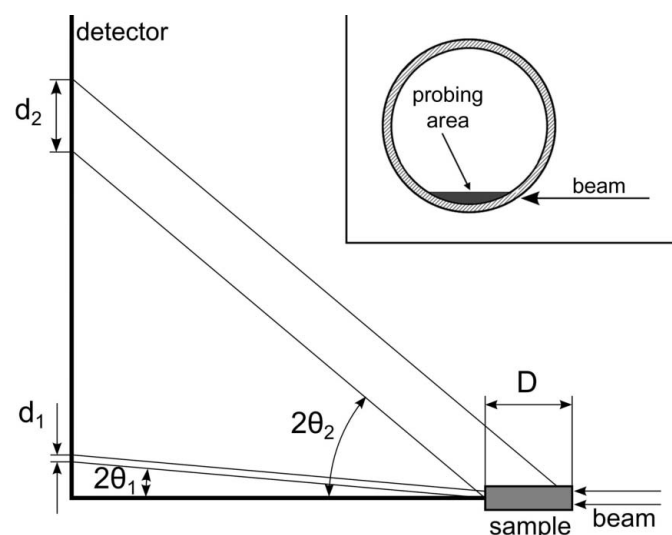


**Figure 2**

Effect of the sample thickness (along the beam) on the width of diffraction peaks depending on the  $2\theta$  angle. The inset shows how the sample thickness changes with the position of the beam in standard jars.  $D$  is the sample thickness;  $d_1$  and  $d_2$  are the projections of the sample on the detector at diffraction angles of  $2\theta_1$  and  $2\theta_2$ , respectively.

## 2. Experimental

### 2.1. 3D printing of the jars

The three-dimensional model jar drawings were first created in the *KOMPAS-3D* CAD software (ASCON, 2013). These models were further processed, including slicing and Gcode generation, in the *MakerBot Desktop Beta* software (MakerBot Software Team, 2014). The supporting information contains a zip file with three-dimensional models of all jars mentioned in the article available in STEP (supported by most CAD and CAM software) and STL (can be directly used for 3D printing) formats. The jars were printed by a dual extruder from a FLASHFORGE printer that prints the objects by depositing layers of plastic. This technique is called fused deposition modelling. The printer, equipped with 0.4 mm-diameter nozzles, has a layer resolution, *i.e.* the thickness of a layer, of 0.1 mm. The layers were printed perpendicularly to the jar symmetry axis in order to reduce delayering due to the shear forces generated by the movement of the milling media.

A colourless thermoplastic made of polylactic acid (PLA) was used as the main material to produce jars. A polyvinyl alcohol polymer was used as a supporting material for more intricate designs, and was later removed by dissolving it in water. Other plastics were also tested, such as acrylonitrile butadiene styrene (ABS) and two coloured PLAs (white and blue). However, their characteristics do not satisfy our criteria for the optimal jar material. The ABS plastic is more brittle than PLA and not robust enough for more sophisticated designs that contain thinner elements. The two coloured PLAs give impurity diffraction peaks from colorants that can interfere with the diffraction peaks of the studied sample and complicate the processing of data.

### 2.2. Jar designs

Among the five different printed jar designs, the first type (*type 1*, Figs. 3a and 3b) was a 3D-printed copy in PLA and ABS of the jar design used by Friščić's team (Halasz, Kimber *et al.*, 2013), named here *type 0*, machined in polymethyl methacrylate (PMMA). These jars have the same dimensions as the metal jars supplied by the shaker mill manufacturer Retsch. We modified the initial jar (Fig. 3a) by making the body and the cap asymmetric, so that the main part of the jar (body) becomes longer and the remaining cap becomes shorter (see Fig. 3b). This gives uniformity to the different jar designs, *i.e.* allows one to use the same caps with the different types of jars.

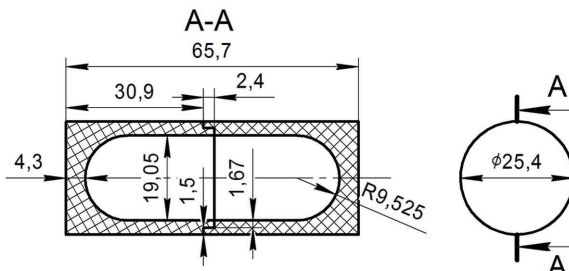
*Thin-walled jar (type 2).* These jars kept the general design of type 0 with a thinner wall thickness. Two modifications were printed: the whole jar having thinner walls (type 2a), and only the side exposed to the X-rays having smaller thickness (type 2b, see Fig. 3c). The thinner wall of type 2a reduces substantially the strength of the jar, whereas the type 2b jars allow for reduced absorption of X-rays while the mechanical strength stays almost the same.

*Thin-walled jar with a groove (type 3).* This is a jar with an inner groove having a width smaller than the diameter of the milling balls. This groove has substantially thinner walls, as it is not subjected to the mechanical impact. The incoming X-ray

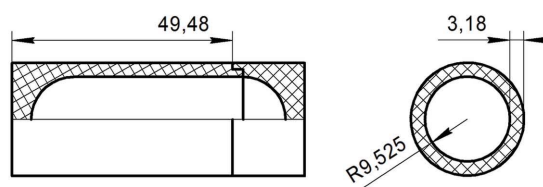
beam hits only the part of sample that is located in the groove (see Fig. 3d).

*Two-chamber jar (type 4).* The last design implements the idea of a jar with two connected chambers: one for milling and another for diffraction. The first chamber where the material is milled is made with thick walls which easily withstand the mechanical impact. The second chamber has thin walls which reduce the background and absorption. If further reduction of

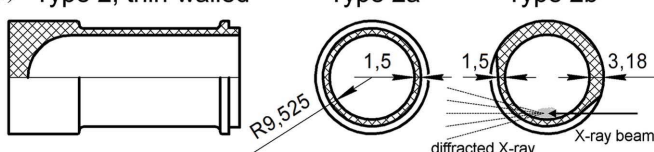
(a) Type 0, basic



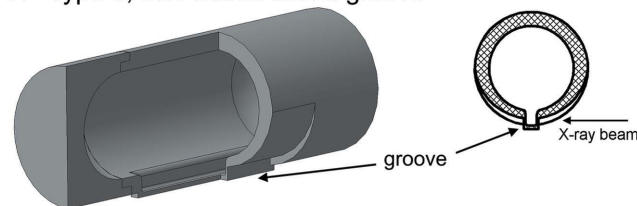
(b) Type 1, long body



(c) Type 2, thin-walled



(d) Type 3, thin-walled with a groove



(e) Type 4, two-chamber

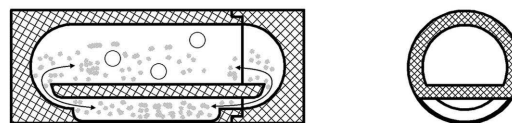


Figure 3

Drawings of the jars. (a) Type 0 jar, basic design from Friščić *et al.* (2013); longitudinal section (left) and end view (right). All necessary dimensions are given here; only those sizes which have been changed are given in all other drawings. (b) Type 1 jar, with joint point near the end of the jar; longitudinal section (left) and cross section (right). (c) Type 2 thin-walled jar; longitudinal section (left), type 2a (middle) and type 2b cross section (right). The paths of incoming and diffracted X-rays are shown schematically for the type 2b cross section. (d) Type 3 thin-walled jar with a groove; isometric view with a cut (left) and cross section (right). (e) Type 4 two-chamber jar; longitudinal section, showing balls and sample separation (left), and cross section (right).

scattering by walls is needed, the plastic wall can be replaced by a thin Kapton film. The size of openings between the two chambers allows only the powder but not the metal balls to pass (see Fig. 3e), removing completely the probability of getting diffraction peaks from the milling balls.

### 2.3. Mechanical tests of the jars

The mechanical resistance of all the jars was tested in the laboratory by loading them with 1 g of NaCl and three stainless steel 5 mm balls in a Retsch MM400 shaker-type mill. The frequency and time of milling were varied, starting from 10 Hz up to 30 Hz (which is the maximum value for the mill) and from the initial 60 s up to the final 6 h ( $4 \times 90$  min). The jars were examined after each stage of the experiment for any damage.

### 2.4. Ball-milling experiments monitored *in situ* by X-ray powder diffraction

The X-ray powder diffraction tests were carried out at the high-energy beamline ID15B (European Synchrotron Radiation Facility, Grenoble, France,  $\lambda = 0.2066$  Å) in a modified MM200 Retsch mill operating at 30 Hz. The first set of tests was conducted using an empty jar of each type and the second set was conducted on jars containing three stainless steel balls (5 mm in diameter) and 250 mg of PbO (as an example of an inorganic material containing a strongly scattering element) or glycine (as an example of an organic material with weak scatterers only). X-ray powder diffraction data were collected using a PerkinElmer 1621 flat-panel detector with a typical exposure time of 10 s. Raw data frames were integrated using Fit2D (Hammersley *et al.*, 1996; Hammersley, 2016). The wavelength, beam centre position and detector distance ( $\sim 1100$  mm) were calibrated using a NIST CeO<sub>2</sub> standard sample. The background for each pattern was subtracted using the Sonneveld–Visser (Sonneveld & Visser, 1975) algorithm implemented in Powder3D (Hinrichsen *et al.*, 2006). Sequential Rietveld refinements were done using the FullProf software package (Rodríguez-Carvajal, 1993).

## 3. Results and discussion

The mechanical resistance criteria should be taken into serious consideration – if a jar collapses or explodes during the running of experiments it could be hazardous or harmful (see photographs of destroyed jars in an *in situ* experiment in the supporting information). Expensive X-ray detectors can be damaged by metal balls or jar fragments or a reacting material; this risk will not be taken by a safety group and may prevent access to a beamline.

The mechanical tests performed in the laboratory on all the 3D-printed jars, types 1 to 4 (including even the thin-walled design of type 2a), show no substantial damage of these jars by the ball impacts compared with the type 0 jar. In type 0 jars made of a monolithic piece of PMMA, the first signs of cracks in the wall induce a fast ageing of the jar, observable after just a few minutes of milling (see Fig. S2 in the supporting infor-

mation). They appear especially early in the presence of solvent such as during liquid-assisted ball-milling experiments. In 3D-printed jars the defects do not grow as the jars are made of plastic threads (similar to high-pressure carbon-fibre bottles) and cracks become localized but do not expand further. The resistance of all of the printed jars is comparable, except potentially for the type 2a jar as the wall is thinner for the whole body.

The scattering from the different types of jars was checked with synchrotron radiation at beamline ID15B. Scattering from the jar material contributes most significantly to the background intensity in real ball-milling experiments; see the

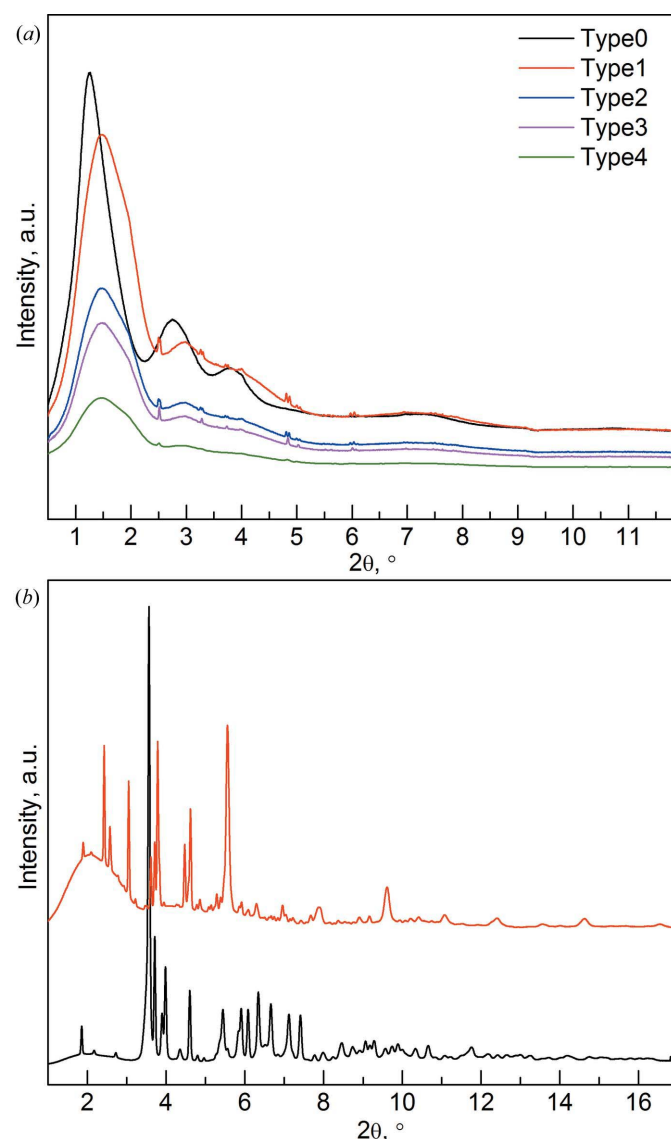


**Figure 4**  
(a) Powder patterns taken on empty jars, showing the background contribution. Minor diffraction peaks originate from a colorant in the plastic. We used coloured PLA in our first test and only later switched to the colourless PLA, which gives only an amorphous contribution to the diffraction patterns. (b) Examples of powder patterns measured *in situ* during the ball-milling experiment in the type 1 jar. The powder pattern of the strongly scattering sample (PbO) is represented by the black line and that of the weakly scattering sample (glycine,  $C_2H_5NO_2$ ) by the red line.

comparison in Fig. 4(a). For the jars of types 0 and 1, having the same geometry but made of a different material (PMMA and PLA, respectively), the shape of the background is different. However, the integral intensities of the background humps are similar as the scattering properties of these materials are comparable. The background from the jars of types 2 and 3 is significantly lower because they have a thinner wall in comparison with the jars of types 0 and 1. As expected, the background intensity for the jar of type 4 is the lowest since the jar walls are the thinnest among the reported jar designs (0.8 mm). After these tests, we modified the jar of type 4 by replacing the plastic (PLA) bottom wall with a piece of Kapton film to obtain the lowest possible background. This modified jar was found to have good working properties, *i.e.* it did not collapse during milling in the laboratory, but was not tested during *in situ* experiments at the synchrotron. Fig. 4(b) shows examples of powder patterns from weakly and strongly scattering samples contained in jars of type 1. We did not subtract background for this pattern to illustrate the quality of the data. Note that even the weakly diffracting sample has a good signal-to-noise and a reasonable signal-to-background ratio.

To study the sampling efficiency of our 3D-printed jars during milling, we needed a simple system in which a reaction occurs at a reasonable speed: not too fast in order to allow us to trace phase changes and not too slow in order not to waste the beam time. So we chose PbO as a model system. PbO has two polymorphs at ambient conditions: tetragonal  $\alpha$ -PbO (known as litharge, red) and orthorhombic  $\beta$ -PbO (known as massicot, yellow), which transform into each other upon a change in temperature and/or pressure, as well as upon mechanical treatment. Both polymorphs of PbO (used as paints) and probably the recipe for their transformation have been known since the ancient Roman era (Bostock & Riley, 1855; Nriagu, 1983; Rapp, 2009). To date, this polymorphic transformation has been extensively studied under various conditions, including ball milling (Clark & Rowan, 1941; Senna & Kuno, 1971; Staszewski *et al.*, 2012) (mechanochemical transition induces the transformation of  $\beta$ -PbO to  $\alpha$ -PbO). Both polymorphs of PbO diffract well and give simple diffraction patterns, which make them a perfect model system for testing jars in *in situ* ball-milling experiments. A commercial PbO powder (VWR Chemicals, 98%) that contained only  $\beta$ -PbO, as shown by its diffraction pattern, was used as received. During *in situ* ball-milling experiments, we monitored the conversion of  $\beta$ -PbO into  $\alpha$ -PbO. The dependence of the content of the  $\alpha$  phase on the milling time is shown in Fig. 5. The data show that the 3D-printed jars are well suited for the mechanochemical experiments. Moreover, substantial conversion is achieved within the time frame of a typical milling experiment convenient to follow by diffraction. Note that 100 frames of 10 s allow for an acceptable conversion monitored with a time resolution close to that typically desirable.

The rate of conversion for different jar types differs. However, as we performed only one experiment for each type of jar owing to the limited synchrotron beam time, we think

that the absolute values of the conversion rates should be taken with caution, as they might vary from one experiment to another. The jars of types 0, 1 and 2 have the same internal geometry, so we expect a similar rate; however, they show some spread (the type 0 jar is made of a different material from 1 and 2, which may affect the rate). Surprisingly, type 3 (with a groove) shows the same rate of conversion as type 0 despite the difference in shape and material. Type 4 demonstrates the lowest conversion rate, which is to be expected for a jar with two chambers: at each moment, only a part of the sample in the upper chamber is milled, while the other part is measured in the bottom chamber; the mixing between the two chambers is slowed down in comparison with jars having one volume. Nevertheless, in the type 4 jar, the amount of the  $\alpha$  phase continues to grow, demonstrating the operability of this design. We stress that the background from the type 4 jar is the smallest (see Fig. 4a) and also that the metallic balls are physically not able to come across the primary X-ray beam.

Although all the tested jars showed good efficiency, the main drawback of the type 3 and 4 jars is that they are not suitable for LAG experiments. In practice, wet powders easily stick inside the narrow parts of the jars and thus the material exposed to X-rays is not taking part in the reaction.

Since we used hard radiation in our tests ( $\lambda = 0.2066 \text{ \AA}$ ), the geometry of the jars did not alter significantly the broadening of the diffraction peaks (see Fig. 2 and §1). Thus, we cannot affirmatively conclude whether these jar designs help to reduce the FWHM of the peaks at higher angles. However, we see the type 3 thin-walled jars with a groove as the most promising for measurements at low-energy beamlines aiming for relatively high angular resolution: the thin-walled groove contains the sample within a small volume, providing both for a low background/absorption and for higher resolution in the reciprocal space.

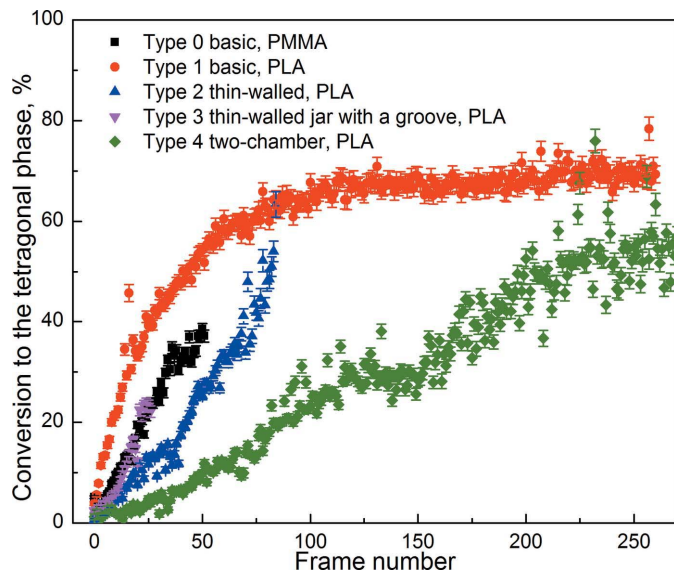


**Figure 5**  
Weight fraction of the tetragonal  $\alpha$ -PbO phase as a function of ball-milling time for the different types of jars. The data were taken over a time interval of 10 s per frame.

## 4. Conclusion

*In situ* observation of a mechanochemical reaction by X-ray powder diffraction offers multiple possibilities to researchers in the field, to access previously unattainable information from a ball-milling process. There have been many developments in this method; however, no real improvements in the essence of the technique, *i.e.* the quality of the X-ray diffraction patterns, have been achieved up to now. We have shown that 3D printing is an easily accessible way to produce milling jars optimized for improved background, absorption and angular resolution in X-ray powder diffraction experiments. The 3D-printed PLA jars show good mechanical strength and are suitable for ball-milling experiments; they are also more resistant to solvents compared with PMMA. 3D printing allows for low-cost fast production on demand. As an example, our team has travelled to the ESRF with a 3D printer, producing the jars during a synchrotron experiment. Further developments in this direction are needed to exploit fully all the information brought by this promising methodology, especially at moderate-energy beamlines aiming for high-resolution data. The source files for printing the jars are available as supporting information.

## Acknowledgements

We are grateful to Ivan Halasz and Tomislav Friščić for providing the modified ball mill for our *in situ* experiments at ID15B. The authors thank FNRS for financial support and the ESRF for beamtime allocation at ID15B. We acknowledge the Fonds Speciaux de Recherche (UCL) for the incoming post-doctoral fellowship cofunded by the Marie Curie actions of the European Commission granted to NT. We thank Elena Boldyreva and Nicola Casati for fruitful discussion and helpful advice, Ivan Tumanov for the photographs of the destroyed jars of type 0, and Pavel Sulimenko for the tips about 3D-printing settings.

## Funding information

Funding for this research was provided by: Fonds De La Recherche Scientifique – FNRS (award No. CC 1.5169.12, PDR T.0169.13, EQP U.N038.13).

## References

- ASCON (2013). *KOMPAS-3D V13*. ASCON Group, St Petersburg, Russian Federation.
- Batzdorf, L., Fischer, F., Wilke, M., Wenzel, K.-J. & Emmerling, F. (2015). *Angew. Chem. Int. Ed.* **54**, 1799–1802.
- Boldyreva, E. (2013). *Chem. Soc. Rev.* **42**, 7719–7738.
- Bostock, J. & Riley, H. T. (1855). *The Natural History, Pliny the Elder*. London: Taylor and Francis.
- Casas, L. & Estop, E. (2015). *J. Chem. Educ.* **92**, 1338–1343.
- Chen, T.-H., Lee, S., Flood, A. H. & Miljanić, O. Š. (2014). *CrystEngComm*, **16**, 5488–5493.
- Clark, G. L. & Rowan, R. (1941). *J. Am. Chem. Soc.* **63**, 1302–1305.
- Fischer, F., Heidrich, A., Greiser, S., Benemann, S., Rademann, K. & Emmerling, F. (2016). *Cryst. Growth Des.* **16**, 1701–1707.
- Fischer, F., Lubjuhn, D., Greiser, S., Rademann, K. & Emmerling, F. (2016). *Cryst. Growth Des.* **16**, 5843–5851.
- Friščić, T., Halasz, I., Beldon, P. J., Belenguer, A. M., Adams, F., Kimber, S., Honkimäki, V. & Dinnebier, R. E. (2013). *Nat. Chem.* **5**, 66–73.
- Gracin, D., Štrukil, V., Friščić, T., Halasz, I. & Užarević, K. (2014). *Angew. Chem. Int. Ed.* **53**, 6193–6197.
- Halasz, I., Kimber, S. A. J., Beldon, P. J., Belenguer, A. M., Adams, F., Honkimäki, V., Nightingale, R. C., Dinnebier, R. E. & Friščić, T. (2013). *Nat. Protoc.* **8**, 1718–1729.
- Halasz, I., Puškarić, A., Kimber, S., Beldon, P. J., Belenguer, A. M., Adams, F., Honkimäki, V., Dinnebier, R. E., Patel, B., Jones, W., Štrukil, V. & Friščić, T. (2013). *Angew. Chem. Int. Ed.* **52**, 11538–11541.
- Hammersley, A. P., Svensson, S. O., Hanfland, M., Fitch, A. N. & Hausermann, D. (1996). *High Pressure Res.* **14**, 235–248.
- Hammersley, A. P. (2016). *J. Appl. Cryst.* **49**, 646–652.
- Hinrichsen, B., Dinnebier, R. E. & Jansen, M. (2006). *Z. Kristallogr. Suppl.* **23**, 231–236.
- Huot, J., Ravnsbaek, D. B., Zhang, J., Cuevas, F., Latroche, M. & Jensen, T. R. (2013). *Prog. Mater. Sci.* **58**, 30–75.
- Kitson, P. J., Macdonell, A., Tsuda, S., Zang, H., Long, D.-L. & Cronin, L. (2014). *Cryst. Growth Des.* **14**, 2720–2724.
- MakerBot Software Team (2014). *MakerBot Desktop Beta*. MakerBot Industries, LLC, Brooklyn, NY, USA.
- Margetic, D. & Štrukil, V. (2016). *Mechanochemical Organic Synthesis*. Amsterdam: Elsevier Science.
- May, P. A. & Moore, J. S. (2013). *Chem. Soc. Rev.* **42**, 7497–7506.
- Nriagu, J. O. (1983). *Lead and Lead Poisoning in Antiquity*. New York, Chichester, Brisbane: John Wiley and Sons.
- Ralphs, K., Hardacre, C. & James, S. L. (2013). *Chem. Soc. Rev.* **42**, 7701–7718.
- Rapp, G. (2009). *Archaeomineralogy*. Berlin, Heidelberg: Springer.
- Rodríguez-Carvajal, J. (1993). *Phys. B Condens. Matter.* **192**, 55–69.
- Scalfani, V. F. & Vaid, T. P. (2014). *J. Chem. Educ.* **91**, 1174–1180.
- Senna, M. & Kuno, H. (1971). *J. Am. Ceram. Soc.* **54**, 259–262.
- Sonneveld, E. J. & Visser, J. W. (1975). *J. Appl. Cryst.* **8**, 1–7.
- Staszewski, M., Myczkowski, Z., Bilewska, K., Lis, M. & Czepelak, M. (2012). *J. Achiev. Mater. Manuf. Eng.* **52**, 39–46.
- Užarević, K., Halasz, I. & Friščić, T. (2015). *J. Phys. Chem. Lett.* **6**, 4129–4140.
- Wang, G.-W. (2013). *Chem. Soc. Rev.* **42**, 7668–7700.
- Zhu, S.-E., Li, F. & Wang, G.-W. (2013). *Chem. Soc. Rev.* **42**, 7535–7570.